New mechanism of fibronectin fibril assembly revealed by live imaging and super-resolution microscopy.

Darshika Tomer[1], Sudipto Munshi[2], Brianna E. Alexander[1,3], Brenda French[2], Pavan Vedula[4], Andrew House[5], Murat Guvendiren[5], Anna Kashina[4], Jean E. Schwarzbauer[6], and Sophie Astrof[1,*].

1. Department of Cell Biology and Molecular Medicine, Cardiovascular Research Institute, Rutgers Biomedical and Health Sciences, 185 South Orange Ave, Newark, NJ, 07103, USA.

2. Sidney Kimmel Medical College of Thomas Jefferson University, Philadelphia, PA, 19107, USA

3. Multidisciplinary PhD Program in Biomedical Sciences. Cell Biology, Neuroscience and Physiology track, Rutgers Biomedical and Health Sciences, Newark, NJ, 07103, USA.

4. Department of Biomedical Sciences, University of Pennsylvania, Philadelphia, PA 19104, USA

5. Otto H. York Chemical and Materials Engineering, Department of Biomedical Engineering, New Jersey Institute of Technology, Newark, NJ 07102, USA

6. Department of Molecular Biology, Princeton University, Princeton, New Jersey, USA

*Author for correspondence: Sophie Astrof, Ph.D.
Phone: 617-429-8295
E-mail: sophie.astrof@rutgers.edu

Abstract

Fibronectin (Fn1) is an essential ECM glycoprotein important for embryonic development and homeostasis. The functions of Fn1 in regulating cell fate decisions, morphogenesis and cellular responses to injury are intimately linked to the process of Fn1 fibrillogenesis. Therefore, understanding the mechanisms by which Fn1 proteins assemble into fibrils is necessary to gain insights into diverse functions of Fn1. Using CRISPR/Cas9 mutagenesis, we generated mice and cell lines wherein a sequence encoding a fluorescent protein (FP) was knocked into the *Fn1* locus replacing the termination codon, resulting in the expression of Fn1-FP proteins subject to endogenous regulation. Live imaging and super-resolution microscopy revealed that Fn1 fibrils are not continuous fibers as was thought before, instead, they are comprised of a discontinuous array of small nanodomains. Live imaging showed that Fn1 nanodomains are mobile and that they become arranged into progressively longer linear arrays as they move toward the nucleus in parallel with the rearward actin flow. The organization of Fn1 nanodomains into linear fibrillar arrays but not the formation of Fn1 nanodomains is regulated by the interactions mediated by the Fn1 N-terminal assembly domain. The nanodomain architecture of Fn1 fibrils is observed in multiple contexts: in three-dimensional ECM *in vivo*, on substrata of different composition and stiffness, and is retained when the linkage of Fn1 fibrils to cells is disrupted. The modular assembly and structure of Fn1 fibrils bears important implications for mechanisms of ECM remodeling and signal transduction.

52 **Introduction**

53 Fibronectin (Fn1) is a requisite component of extracellular matrix (ECM) necessary for
54 embryogenesis and homeostasis (Schwarzbauer and DeSimone, 2011). It is noteworthy that in
55 the absence of Fn1 fibrillogenesis, the binding of Fn1 to cells is not sufficient to regulate key
56 biological processes including those governing embryonic development, angiogenesis,
57 vascular remodeling, or cartilage condensation (Chiang et al., 2009; Rozario et al., 2009;
58 Singh and Schwarzbauer, 2014; Zhou et al., 2008). Therefore, understanding the mechanisms
59 by which Fn1 proteins assemble into macromolecular fibrils is essential to gain insights into *in*
60 *vivo* functions of Fn1. Fn1 fibrillogenesis occurs following the binding of secreted Fn1
61 homodimers to cell-surface integrins. Following integrin binding, intracellular cytoskeletal
62 forces such as actomyosin contractility acting through integrins generate pulling forces on Fn1
63 dimers, exposing epitopes that promote Fn1 fibrillogenesis (Chernousov et al., 1987; Smith et
64 al., 2007; Zhang et al., 1994; Zhang et al., 1997; Zhong et al., 1998). At the cell biological
65 level, the process of Fn1 fibrillogenesis is correlated with the formation of fibrillar adhesions,
66 whereby mobile adhesions containing Fn1 and integrin $\alpha5\beta1$ translocate toward the nucleus
67 resulting in elongated linear arrays termed focal and fibrillar adhesions, containing both Fn1
68 and intracellular cytoplasmic effectors linking Fn1 and actin cytoskeleton (Geiger et al., 2001;
69 Geiger and Yamada, 2011; Lu et al., 2020; Pankov et al., 2000; Zamir et al., 1999; Zamir et al.,
70 2000).

71 It has been thought that Fn1 fibrils arise following partial unfolding and alignment of Fn1
72 dimers in a periodic end-to-end fashion of alternating N- and C-termini, forming continuous
73 fibers (Chen et al., 1997; Dzamba and Peters, 1991; Fruh et al., 2015). However, this model is
74 based on the analyses of fixed samples and electron microscopy wherein the exact
75 composition of the fibrous material imaged could not be easily determined. To evaluate the
76 process of fibrillogenesis in real time, we adopted a CRISPR/Cas9-mediated mutagenesis

77 approach to generate fluorescently-labeled Fn1, subject to physiological regulation of
78 expression and splicing. This approach has enabled us to visualize the initiation and
79 progression of Fn1 fibrillogenesis over an extended period of time. Using live imaging and
80 super resolution microscopy, we uncovered an unexpected mechanism of Fn1 fibrillogenesis.
81 Our data demonstrate that Fn1 fibrils are composed of centripetally-moving Fn1 nanodomains
82 originating at cell periphery. As Fn1 nanodomains move toward the nucleus, they become
83 arranged into progressively longer and longer arrays wherein nanodomains containing a high
84 number of Fn1 dimers alternate with regions containing low or no Fn1. We show that the N-
85 terminal Fn1 assembly region is not required for the formation of Fn1 nanodomains or their
86 centripetal translocation. Instead, the N-terminus of Fn1 regulates the organization of Fn1
87 nanodomains into linear arrays. This model of fibrillogenesis integrates the process of
88 fibrillogenesis with adhesion maturation and provides significant new insights into the
89 mechanisms of ECM formation,
90 remodeling, and signaling.
91

92 **Results**

93 While examining Fn1^{+} ECM by
94 confocal immunofluorescence microscopy
95 in mouse embryos, we observed that Fn1
96 fibrils appeared discontinuous (**Fig. 1a-b**,
97 arrows), containing regularly-spaced
98 regions of high and low fluorescence
99 intensity (**Fig. 1c, Movie 1**; *Movie legends*
100 *are at the end of the manuscript*). This
101 suggested that Fn1 fibrils consisted of
102 regions with a high number of Fn1 dimers

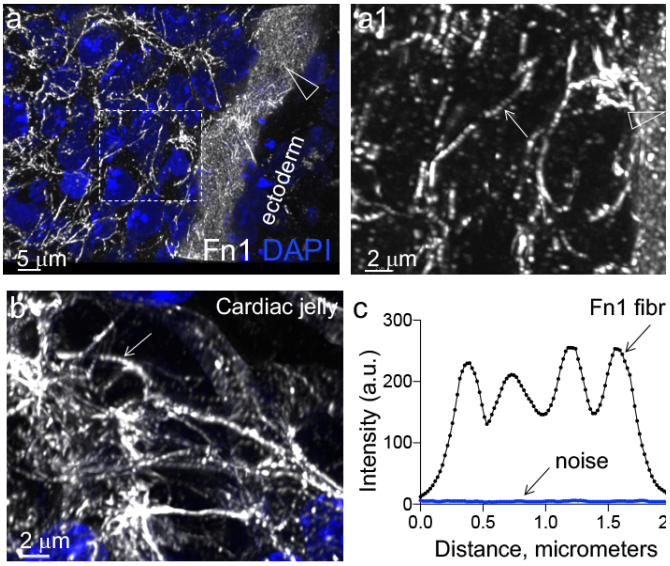

Figure 1. Beaded architecture of Fn1 fibrils in embryonic ECM. Wild-type E9.5 mouse embryos were fixed and stained with the monoclonal antibody to Fn1 (white) and DAPI, and imaged using 100x oil objective, N.A. 1.49, pinhole 0.8, and sampling rate of 40 nm/pixel. **a – a1.** Sagittal optical section through the first pharyngeal arch and **b.** the cardiac jelly, an ECM-rich region between the myocardial and endocardial layers of the outflow tract of the heart. Large arrowheads in **a – a1** point to the ECM at the ectoderm-mesenchyme boundary of the 1st pharyngeal arch. The box in **(a)** is expanded in **a1** to show the beaded Fn1 microarchitecture. Arrow in **a1** points to Fn1 fibril within the arch mesenchyme; **b.** Beaded architecture of Fn1 fibrils in cardiac jelly, e.g., arrow. **c.** Intensity profile plot of a Fn1 fibril shows a regularly-undulating profile, with peaks corresponding with Fn1 "beads"; a.u. arbitrary units.

separated by regions containing a low number of Fn1 dimers (**Fig. 1c**). To test this hypothesis and to determine mechanisms regulating the formation of Fn1 fibrils, we employed a CRISPR/Cas9 knock-in strategy to modify the endogenous Fn1 locus by replacing the termination codon of Fn1 with a sequence encoding a fluorescent protein. This strategy has allowed to generate fluorescently-labeled Fn1 proteins subject to endogenous regulation (**Sup. Fig. 1a-b**), and enabled extended live imaging of Fn1 fibrillogenesis. Using this strategy, we obtained multiple independent lines of mouse embryo fibroblasts (MEFs) expressing Fn1-mEGFP, Fn1-mScarlet-I, Fn1-Neon Green, or Fn1-tdTomato fusion proteins (FP) generated by CRISPR/Cas9-mediated insertion. Western blots showed that FP fusions to Fn1 were specific: FPs were only fused to Fn1 as no other FP fusions were detected either by western blotting or immunofluorescence (IF) (**Sup. Fig. 2a-b**).

Deoxycholate (DOC) insolubility of Fn1 ECM is a classical biochemical assay for proteins stably incorporated into the assembled ECM (Choi and Hynes, 1979; McKeown-Longo and Mosher, 1983; Singh et al., 2010; Wierzbicka-Patynowski et al., 2004). DOC assays demonstrated that the incorporation of Fn1-FPs into ECM was indistinguishable from wild-type, untagged Fn1 (**Sup. Fig. 2c**). To determine whether Fn1-FP proteins carried out the physiological functions of Fn1, we generated $Fn1^{mEGFP}$ knock-in mice. $Fn1^{mEGFP/mEGFP}$ homozygous knock-in animals are viable and fertile (**Sup. Fig. 1b** panels 4 and 5). Furthermore, Fn1-mEGFP proteins were expressed in the same pattern as total Fn1 protein (**Sup. Fig. 2d**) (Peters and Hynes, 1996). Together, these studies demonstrated that Fn1-FP fusion proteins are suitable reagents for investigating mechanisms of Fn1 fibrillogenesis.

To visualize the process of fibrillogenesis in real time, we plated $Fn1^{mEGFP/+}$ MEFs on gelatin-coated cover glass and imaged cells 16 hours after plating using total internal reflection (TIRF) microscopy at the critical angle of incidence. These experiments showed that Fn1 fibrillogenesis initiated at cell periphery as distinct bright Fn1 densities that moved centripetally in parallel with F-actin and aligned into linear arrays of “beads” (arrows in **Movie 2**). TIRF

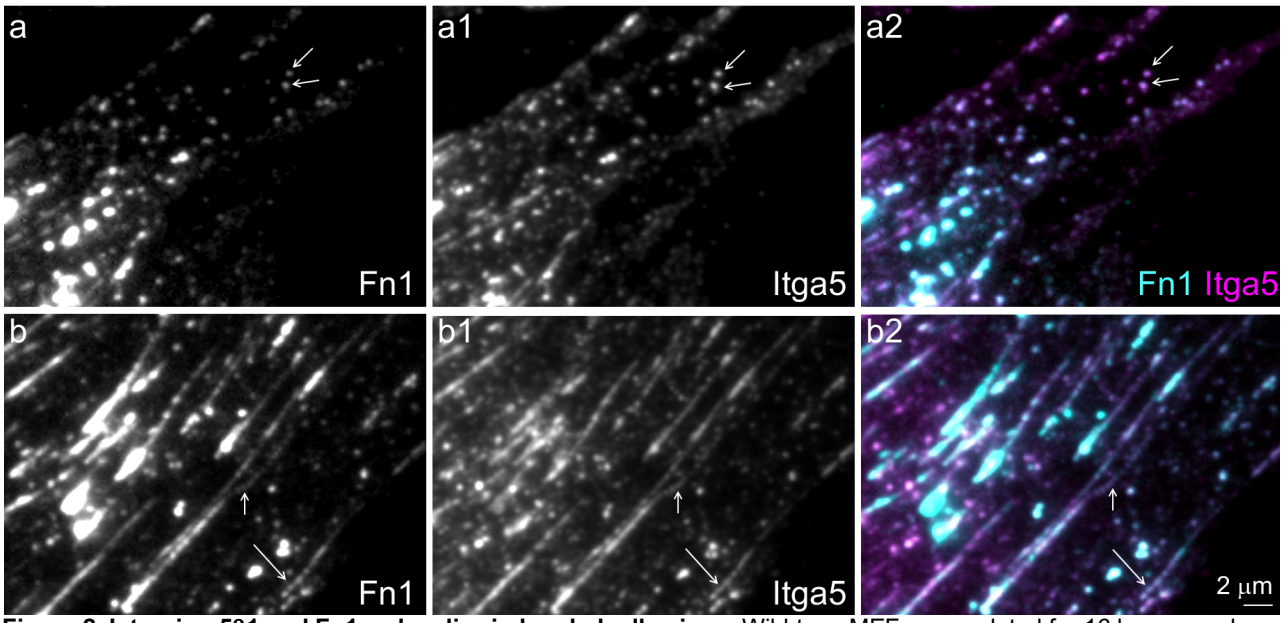

Figure 2. Integrin α5β1 and Fn1 co-localize in beaded adhesions. Wild-type MEFs were plated for 16 hours on glass coverslips, then fixed, stained with antibodies to Fn1 and integrin α5 (Itga5), and imaged at the critical angle of incidence using 100x oil objective, NA 1.49. **a – a2** cell periphery. Arrows in **a-a2** point to examples of non-fibrillar Fn1 adhesions ("beads") at cell periphery. **b - b2** medial portion of a cell containing beaded fibrillar adhesions (arrows). Note that both Itga5 and Fn1 stainings are beaded. Magnifications in all panels are the same.

imaging also showed that the domains of higher fluorescence intensity of Fn1 co-localized with integrin α5β1 both in non-fibrillar adhesions (arrows in **Fig. 2a-a2**) and in fibrillar adhesions (arrows in **Fig. 2b-b2**), and that Fn1 and α5β1 fibrillar adhesions are beaded (**Fig. 2b-b2**, arrows). We also observed the beaded architecture of Fn1 fibrils using an independent imaging method by employing Zeiss Airyscan (**Sup. Fig. 3**). Staining using monoclonal and polyclonal antibodies recognizing distinct and multiple epitopes in Fn1 resulted in the discontinuous appearance of Fn1 fibrils (**Fig. 3a1-c1**). Fn1 fibrils formed by cells plated on glass, gelatin, laminin 111 or vitronectin were beaded Fn1 fibrils (**Fig. 3**, and **Sup. Figs. 3-4**), and so were Fn1 fibrils in cell-free areas (**Fig. 3a, a1**) and between cells (**Fig. 3b-c**). In addition, the beaded appearance of Fn1 fibrils was observed when cells were plated on soft substrata such as hydrogels of variable stiffness (**Sup. Fig. 4c-d**). In the latter experiment, Fn1 was detected by imaging the native fluorescence of Fn1-mEGFP, indicating that the beaded

appearance of Fn1 fibrils was independent of antibody staining. Taken together, these studies indicated that the beaded appearance of Fn1 fibrils was a general feature of Fn1 ECM seen in 3D ECM *in vivo* and under different conditions *in vitro*.

To test the hypothesis that the "beads" in Fn1 strings were contiguous, cultures were treated with 2% DOC. 2% DOC treatment dissolves cell membranes and cytoplasmic components, leaving insoluble ECM devoid of cell contact (see **Movie 3** for time-laps of dissolution of cellular components, F-actin and DNA). This experiment showed that Fn1 fibrils in assembled ECM retained their beaded architecture in the absence of cell contact (**Fig. 3d**). Together, these data indicated that the beaded topology of Fn1 fibrils is a feature of physiological three-dimensional Fn1 ECM *in vivo* and suggested that the beads are contiguous.

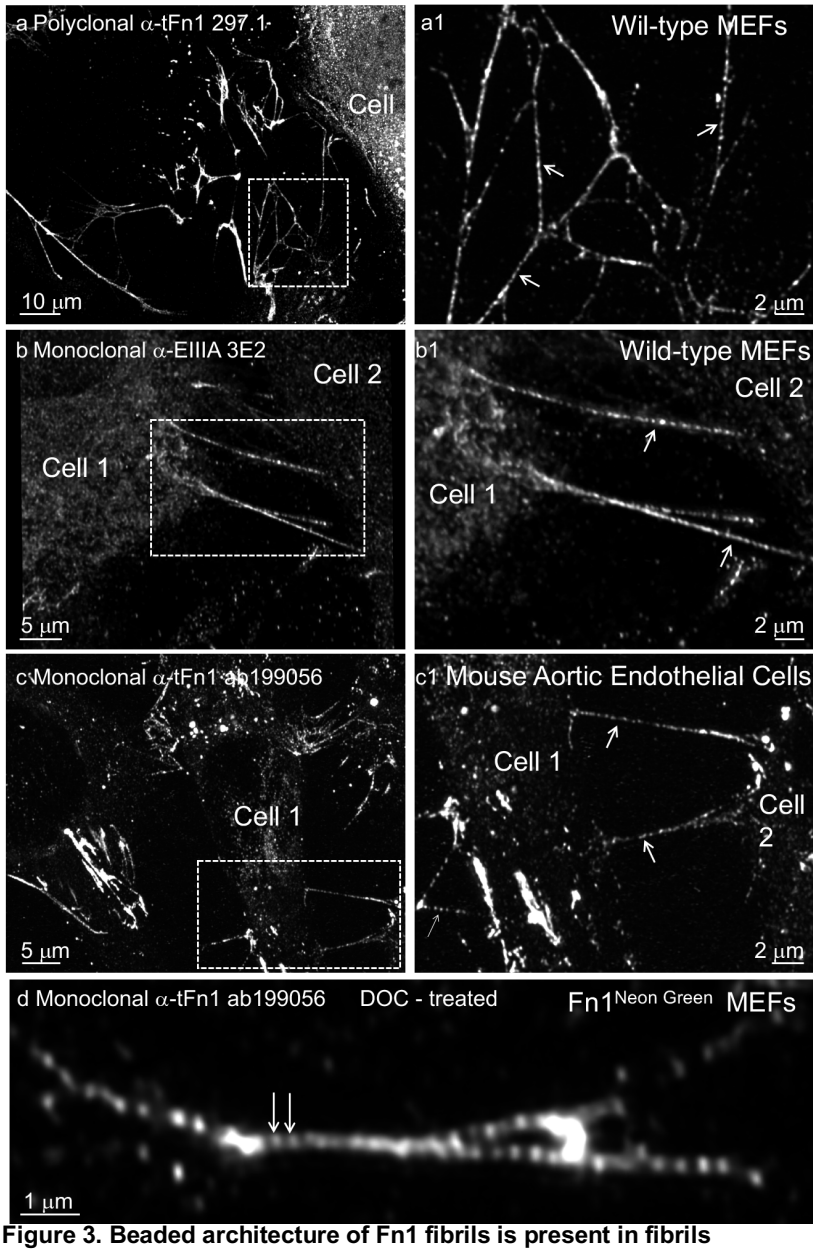

Figure 3. Beaded architecture of Fn1 fibrils is present in fibrils between cells and is retained in the absence of cell contact. a-b. Fn1 secreted by wild-type MEFs and deposited **a)** on glass or **b)** between cells. **c.** Fn1 fibrils between endothelial cells. Boxes in **a – c** are magnified in **a1-c1**. Arrows point to fibrils left behind on substrata (**a1**) or between cells (**b1-c1**). **d.** $Fn1^{Neon\ Green}$ MEFs were treated with 2% DOC pH 8 until cells were dissolved (see Movie 3). Following DOC treatment, Fn1 was imaged using 100x oil objective, NA 1.49, pinhole size 0.8 Airy units, and sampling resolution of 40 nm/pixel in x,y. Note beaded architecture (arrows).

166 To determine the relationship between the beaded architecture of Fn1 seen by
167 diffraction-limited microscopy with Fn1 nanoarchitecture, we plated Fn1$^{mEGFP/+}$ MEFs on glass
168 for 16 hours, then fixed and stained cells using a monoclonal antibody to the central region of
169 Fn1. Fn1-mEGFP fluorescence was imaged in the TIRF mode at the critical angle of incidence,
170 while the binding of the monoclonal αFn1 antibody was detected with Alexa Fluor-647-
171 conjugated secondary antibody and imaged by Stochastic Optical Reconstruction Microscopy
172 (STORM). STORM was performed by illuminating samples at the critical angle of incidence, as
173 described in (Jimenez et al., 2020). Thin beaded fibrillar adhesions (arrow in **Fig. 4a**) were
174 resolved by STORM (**Fig. 4b-b2**) to be arrays of regularly-spaced nanodomains that were

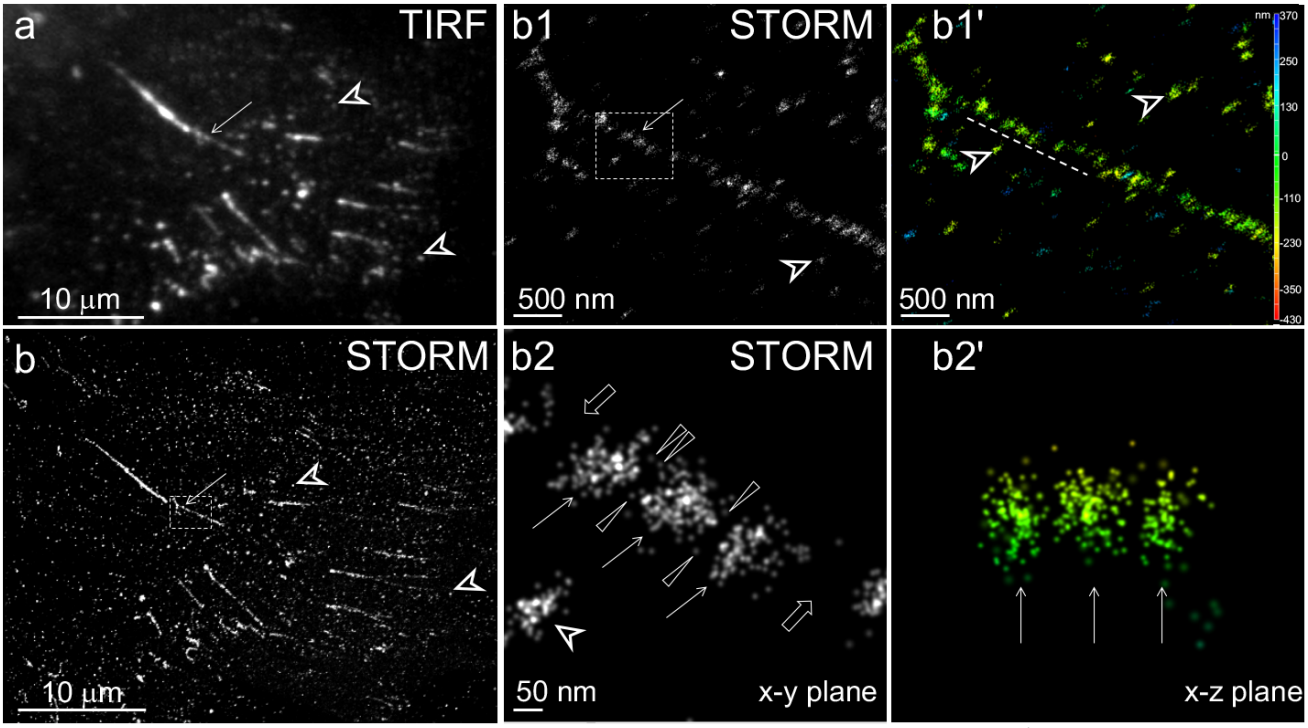

Figure 4. Fn1 fibrils are composed linear arrays of Fn1 nanodomains. Fn1$^{mEGFP/+}$ MEFs were plated on glass for 16 hrs, then fixed and stained with antibodies to GFP followed by secondary antibodies conjugated to Alexa-647. **a.** Native GFP fluorescence imaged by TIRF using 100x objective NA 1.49. Arrow in **a** points to a thin, beaded Fn1 fibril resolved by STORM in **b1, b1'** and **b2. b.** The entire field of view in **a** is imaged by STORM detecting Alexa-Fluor 647-conjugated antibody (see Methods). The box in **b** is expanded in **b1**. The box in **b1** is expanded in **b2**. The arrow in **b1** points to the same region as the arrow in **a**. Arrows in **b2** point to Fn1 nanodomains; arrowheads point to Fn1 localizations between the nanodomains, notched arrowheads point to Fn1 nanodomains that are not in fibrils and wide arrows point to Fn1-free areas between the nanodomains in the fibril marked by the arrow in **a**. **a, b, b1, b1'** and **b2** are in x-y planes; **b2'** shows the nanodomains in **b2** in the x-z plane. Images in **b1'** and **b2'** are depth-coded according to the scale in **b1'**. See Movie 4 for 3D rotation of the fibril underlined in **b1'** around the x-axis.

175 symmetrical in x, y, and z dimensions (**Fig. 4b1, b2, b2'** and **Movie 4**). The space between
176 nanodomains contained a few or no Fn1 localizations (**Fig. 4b2** and **Movie 4**).
177 Fn1 is a large, multi-domain, ~250 kDa glycoprotein secreted as a homodimer, wherein
178 Fn1 subunits are linked in the anti-parallel orientation by two di-sulfide bonds at their C-termini
179 (Schwarzbauer and DeSimone, 2011; Skorstengaard et al., 1986). To investigate the
180 relationship between the domain structure of Fn1 protein and the nanodomain architecture of
181 Fn1 fibrils, we used antibodies to distinct parts of Fn1 protein (depicted in **Model 1** at the
182 bottom of **Fig. 5**,) and STORM. For these experiments, wild-type and Fn1$^{mEGFP/+}$ MEFs were
183 sparsely-plated in Ibidi 8-well glass-bottom chambers overnight, allowing to observe the
184 structure of thin fibrils. Cells were then fixed and stained with antibodies recognizing different
185 Fn1 epitopes: polyclonal rabbit antibodies raised to recognize the first six type III repeats of
186 Fn1 (Fn1 III_{1-6}) (Vega et al., 2020) (**Fig. 5** column 1), a monoclonal antibody recognizing an
187 epitope within the central region of Fn1 (**Fig. 5** columns 2, 4-5), polyclonal anti-serum 297.1
188 raised against the entire Fn1 protein (Rickelt and Hynes, 2018) (**Fig. 5**, column 3), or
189 polyclonal antibodies to GFP, recognizing the C-terminus of Fn1-mEGFP protein (**Fig. 6**,
190 column 5). To maximize the labeling density, the polyclonal anti-Fn1 III_{1-6} and 297.1 antisera
191 were used at a 40- and 4-fold higher concentrations than for routine immunofluorescence
192 microscopy, respectively. Together with the use of excess secondary antibodies each
193 conjugated to 3 – 6 molecules of Alexa-647, this approach maximizes the chance that all the
194 epitopes recognized by the 1° antibodies will be localized by STORM (Jimenez et al., 2020).
195 We first focused on the analyses of thin Fn1 fibrils like those marked by the arrows in
196 (**Fig. 4a-b**) to study the initiation of fibril formation rather than fibril bundling or branching. Each
197 antibody resulted in the detection of long characteristic Fn1 fibrils (**Fig. 5a-c**). Successive
198 magnifications show that independent of the antibody used for staining, Fn1 fibrils contained
199 linear arrays of nanodomains (thin arrows in **Fig. 5d, magnified in 5e**) separated by regions
200 containing a small number or no Fn1 localizations (as in **Fig. 4, Movie 4**).

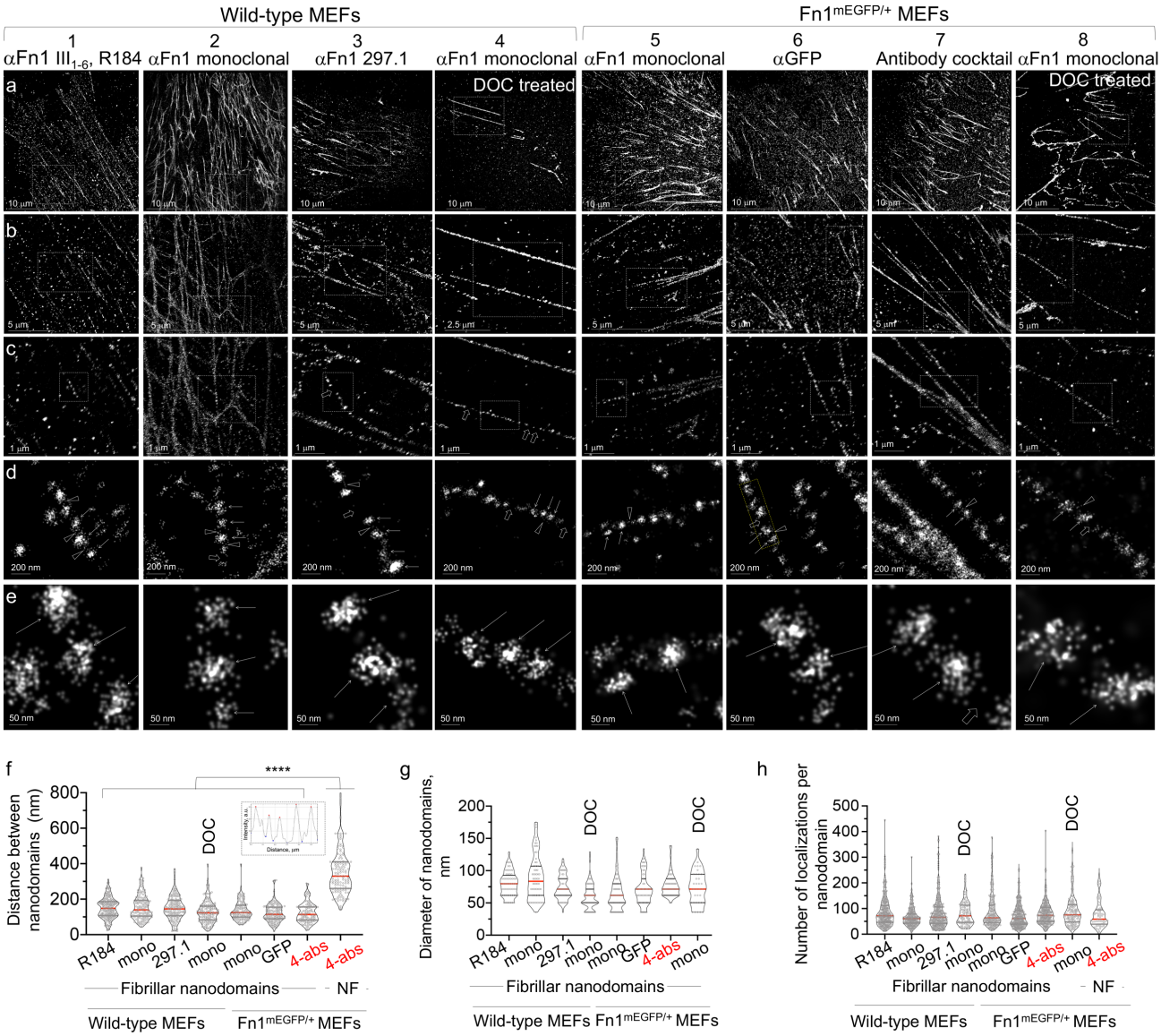

Model 1 Two Fn1 dimers aligned in a periodical end-to-end fashion. If fibrils were composed of periodically aligned dimers, they would be uniformly stained by the antibody cocktail:

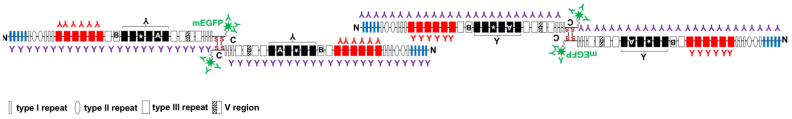

Model 2 Fn1 fibrils form from nanodomains containing multiple Fn1 dimers

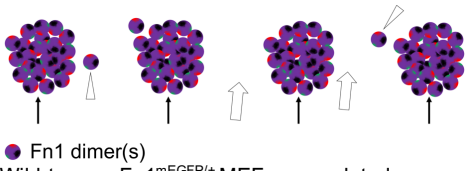

Figure 5. Fn1 fibrils are composed of nanodomains containing multiple Fn1 dimers. Wild-type or Fn1$^{mEGFP/+}$ MEFs were plated on glass for 16 hrs, fixed and stained with different antibodies to Fn1 followed by Alexa 647-conjugated secondary antibodies. Columns showing cells treated with DOC prior to fixation are marked. Cells were imaged using STORM**. a.** zoom-out views to show the overall appearance of Fn1 fibrils. **b-e.** Successive magnifications of fibrils shown in (**a**). Arrows in **d** point to nanodomains magnified in **e;** arrowheads in **d-e** point to Fn1 molecules between nanodomains, wide open arrows point to Fn1-free zones between nanodomains in a fibril. **f.** distances between nanodomains within fibrils or non-fibrillar (NF) nanodomains, **** $p<10^{-4}$, Kruskal-Wallis test, with Dunn's correction for multiple testing. Inset in **f** is a plot profile of the fibril marked by the box in the column **6d** showing regularly-spaced peaks of intensity. DOC-treated samples are marked. 4-antibody cocktail contains four antibodies as in **Model 1**. **g.** Diameter of nanodomains in fibrils. **h.** number of Fn1 localizations per nanodomain in fibrils. **Model 1**. Two Fn1 dimers in a fibril. Depiction of antibody coverage of Fn1 fibrils if dimers were oriented in end-to-end fashion with alternating N- and C-termini. **Model 2.** Our data show that Fn1 fibrils consist of a linear array of nanodomains (black arrows) containing multiple Fn1 dimers (Fn1 dimers are depicted as balls and color-coded according to the antibody scheme in **Model 1**. Arrowheads point to Fn1 and open arrows point to Fn1-free areas between nanodomains.

201

202 Surprisingly, staining with the polyclonal anti-serum 297.1 raised to the entire Fn1 and,
203 presumably, recognizing multiple epitopes along Fn1, resulted in the same pattern of regularly-
204 spaced nanodomains as staining with antibodies recognizing distinct parts of Fn1 molecule
205 (**Fig. 5,** column 3), suggesting that each Fn1 localization contained the entire Fn1 sequence,
206 and that each nanodomain contained multiple Fn1 dimers.
207
208 These data are not consistent with previous models suggesting that Fn1 fibrils are composed
209 of periodically aligned Fn1 dimers arranged in an end-to-end fashion of alternating N- and C-
210 termini (Chen et al., 1997; Dzamba and Peters, 1991; Fruh et al., 2015) (**Model 1** at the
211 bottom of **Fig. 5**). Such periodic alignment of Fn1 dimers necessitates that staining using
212 polyclonal antibodies would result in a uniform labeling of thin Fn1 fibrils, as depicted in **Model**
213 **1.** The dimers in the **Model 1** are aligned in an end-to-end fashion, according to the current
214 Fn1 fibrillogenesis model, with the predicted overlap between the N-terminal Fn1 assembly
215 domain (blue) and the first six type III repeats of Fn1 (red) (Singh et al., 2010)). If Fn1 fibrils,
216 were indeed composed of continuous, linear arrays of dimers, the use of all four depicted in
217 **Model 1** would be predicted to uniformly label Fn1 fibrils.
218
219 To test this prediction, we used $Fn1^{mEGFP/+}$ MEFs and a cocktail of four antibodies recognizing
220 the beginning (αFn1 III_{1-6}), middle- (αFn1 monoclonal), and the end (αGFP) of Fn1-mEGFP
221 protein in addition to all the epitopes recognized by 297.1 polyclonal antibody. The binding of
222 all the antibodies in the cocktail was detected by a cocktail of secondary antibodies that were
223 each conjugated to 3 – 6 molecules of Alexa-647 (**Fig. 5, column 7**). The nanoarchitecture of
224 thin Fn1 fibrils, the nanodomain spacing (124 $\pm$ 25 nm between nanodomains in fibrils, on
225 average), nanodomain size (average diameter 77 $\pm$ 18 nm), and the number of Fn1
226 localizations per nanodomain (average of 80 $\pm$ 43 localizations) detected by the cocktail of four

227 antibodies were indistinguishable from those produced by each type of the antibody
228 individually (**Fig. 5d – e**, quantified in **Fig. 5f-h** and **Tables 1 –3**). These results indicate that
229 Fn1 fibrils are not uniform. Instead, our data show that Fn1 fibrils are arrays of nanodomains
230 containing multiple Fn1 dimers separated by areas containing a few or no Fn1 molecules (**Fig.**
231 **5, Model 2**). The nanoarchitecture of Fn1 fibrils following the treatment with 2% DOC which
232 removes cells and cellular components, was similar to untreated fibrils (**Fig. 5,** columns 4 and
233 8, **Fig. 5f – h**). These data indicate that the nanodomain architecture is a feature of mature
234 Fn1 fibrils.
235
236 Fn1 nanodomains were also present outside of fibrils, we term them non-fibrillar nanodomains
237 (e.g. notched arrowheads in **Fig. 4**). About 3 – 5 such nanodomains are seen as a "bead" in
238 conventional diffraction-limited microscopy. Non-fibrillar Fn1 nanodomains contained a similar
239 number of Fn1 localizations per nanodomain and were of similar size compared with Fn1
240 nanodomains in fibrils (**Fig. 5h, Tables 2 – 3**). Staining using antibodies to endosomal and
241 lysosomal markers (Rab5 and LAMP1) showed no appreciable co-localization with Fn1
242 nanodomains (data not shown). Together with imaging using TIRF microscopy, these findings
243 indicated that Fn1 nanodomains in fibrils and non-fibrillar nanodomains are on the cell surface.
244 Non-fibrillar Fn1 nanodomains were present at cell periphery and throughout the cell surface,
245 but they were not organized into linear arrays and were spaced at an median distance of 329
246 nm (**Table 1**).
247 Live imaging experiments suggested that Fn1 fibrils form from centripetally-translocating
248 Fn1 nanodomains originating at cell periphery (**Movie 2**). To understand the relationship
249 between the observed nanodomain architecture of Fn1 fibrils and the process of fibrillogenesis,
250 we adopted a live imaging approach using $Fn1^{mEGFP/+}$ MEFs and inhibitors of fibrillogenesis.
251 Fn1 fibrillogenesis critically depends on the interactions mediated by the N-terminal assembly
252 domain of Fn1 (domains shaded in blue in **Model 1, Fig. 5**), and inhibitors that interfere with

253 these interactions block the formation of Fn1 fibrils (Filla et al., 2017; Morla et al., 1994;
254 Schwarzbauer, 1991; Sechler et al., 2001; Sechler et al., 1996; Tomasini-Johansson et al.,
255 2001). One such inhibitor is a 49-amino acid peptide derived from *Streptococcus pyogenes*
256 adhesin F1, termed the functional upstream domain (FUD) (Tomasini-Johansson et al., 2001).
257 FUD binds the N-terminal assembly domain of Fn1 and functions as a competitive inhibitor of
258 Fn1-Fn1 interactions (Maurer et al., 2010; Tomasini-Johansson et al., 2001). To determine
259 how N-terminal interactions regulate Fn1 fibrillogenesis, Fn1$^{mEGFP/+}$ MEFs were plated on glass
260 for 4 hours, and then imaged for 15 – 18 hours either in the imaging medium alone, or in the
261 medium containing either 225 nM FUD or 274 nM 11-IIIC, a 68 amino-acid control peptide that
262 does not interfere with Fn1 fibrillogenesis (Morla et al., 1994; Sottile and Chandler, 2005).
263 Untreated cells or cells treated with the control peptide developed and accumulated long Fn1
264 fibrils (**Movie 5**). In contrast, treatment with FUD led to dismantling of the pre-existing Fn1
265 fibrils and inhibited the formation of new Fn1 fibrils (**Movie 6**). Instead of fibrils, cells cultured in
266 the presence of FUD mainly contained centripetally-moving Fn1-mEGFP fluorescent "beads"
267 that only rarely formed strings (**Movie 6**). These experiments suggested that FUD inhibits
268 fibrillogenesis by interfering with the process by which Fn1 "beads" become arranged or
269 connected into linear arrays. To test this hypothesis, Fn1$^{mEGFP/+}$ MEFs were plated for 16 hours
270 in the continuous presence of either 225 nM FUD or 274 nM III-11C control peptides, or were
271 left untreated. Cell were then fixed and stained <u>without permeabilization</u> using monoclonal anti-
272 Fn1 antibodies which were detected with Alexa Fluor 647-conjugated secondary antibodies,
273 and imaged at the critical angle of incidence by STORM at the excitation wavelength of 640
274 nm (Jimenez et al., 2020). This approach abolishes the detection of intracellular Fn1-mEGFP
275 and maximizes the detection of cell-surface Fn1 due to the following: a) the absence of a
276 detergent during fixation, staining and washing, b) detecting the emission of Alexa 647-
277 conjugated antibodies at $\geq$ 670 nm, c) the use of oxygen scavengers in the STORM buffer that
278 inhibits GFP fluorescence (Tsien, 1998), and d) imaging at the critical angle of incidence to

detect fluorescence in close proximity to the plasma membrane. These experiments demonstrated that the organization of nanodomains into linear arrays was lost upon incubation with FUD (compare **Fig. 6a, b, a1, b1** with **Fig. 6c, c1**). Non-fibrillar Fn1 nanodomains in cells treated with FUD had a similar number of Fn1 localizations per nanodomain, and were of similar sizes compared with fibrillar or non-fibrillar Fn1 nanodomains in untreated cells or cells incubated with the control peptide (**Fig. 62-c1-1**, quantified in Fig. **6d** and **Tables 2-3**). Taken together, these data indicate that FUD does not interfere with the formation of Fn1 nanodomains but inhibits the organization of Fn1 nanodomains into linear arrays. Since Fn1 proteins lacking the N-terminal assembly domain do not form fibrils, our experiments suggest

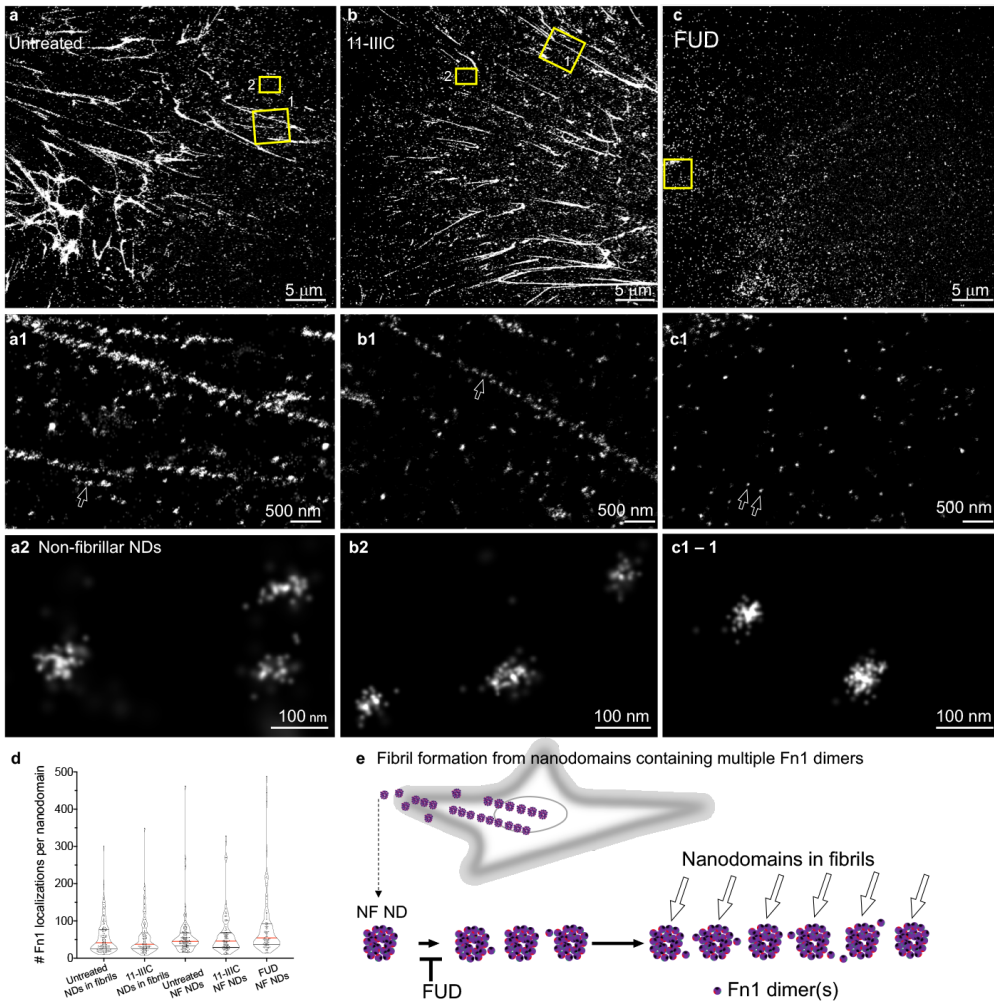

Figure 6. The N-terminal Fn1 assembly domain regulates the organization of Fn1 nanodomains into linear fibrillar arrays. Fn1$^{mEGFP/+}$ MEFs were plated on glass and were either left untreated, or were incubated with the control 11-IIIC peptide, or the FUD peptide for 16 hrs. Cell were then fixed and stained with the monoclonal antibody to Fn1 followed by Alexa 647-conjugated secondary antibodies. Cells were imaged at the critical angle of incidence by STORM. **a – a2**. Untreated, unpermeabilized cells. **b – b2.** Cells incubated with controls 11-IIIC peptide. **c – c1, c1-1** FUD-treated, unpermeabilized cells. Boxes marked 1 in **a-b** were expanded in **a1-b1**. Boxes marked 2 in **a-b**, were expanded in **a2 – b2**. The box in **c** is expanded in **c1** and **c1-1**. Arrows in **a1-b1** point to Fn1 nanodomains (NDs) in fibrils. Arrows in **c1** points to non-fibrillar nanodomains expanded in c1-1; **d.** Quantification of the number of Fn1 localizations in NDs in fibrils and in non-fibrillar NDs after various conditions. Red lines mark medians. Differences are not statistically significant, Kruskal-Wallis test with Dunn's correction for multiple testing. **e.** Model of fibril formation: Fn1 dimers assemble into small nanodomains containing integrin $\alpha5\beta1$ at cell periphery, move rearward with actin flow, and become organized into linear arrays of nanodomains. Joining of the additional Fn1 nanodomains to these arrays leads to the generation of longer fibrils as the assembly moves toward the cell center. FUD does not interfere with the formation of Fn1 nanodomains. But instead, it blocks the organization of Fn1 nanodomains into linear arrays.

304 that interactions mediated by the N-terminal assembly domain of Fn1 are critical for the linking
305 of Fn1 nanodomains into strings.
306
307 **Discussion**
308 In this manuscript, we describe the discovery of a novel mechanism underlying the process of
309 Fn1 fibrillogenesis. We found that the three-dimensional beaded architecture of Fn1 ECM
310 fibrils *in vivo* and in two-dimensional cell culture is due to the presence of Fn1 nanodomains,
311 and showed that each Fn1 nanodomain is composed of multiple Fn1 dimers. Time-laps
312 imaging by confocal and TIRF microscopy showed that Fn1 fibrillogenesis initiated at cell
313 periphery, as bright fluorescent "beads" of Fn1-mEGFP moved centripetally in parallel with F-
314 actin and became organized into linear arrays. Interestingly, the beaded appearance of focal
315 and fibrillar adhesions has been noted before (Zamir et al., 1999; Zamir et al., 2000), and the
316 beaded architecture of cell adhesions can be seen in micrographs from multiple studies (e.g.
317 Fig. 1C in (Zamir et al., 1999), Fig 7a and Sup. Figs 1a and b in (Choi et al., 2008); Fig. 8B in
318 (Damsky et al., 1985); and lower left cell in Fig. 3A (Zhang et al., 2012). However, the
319 significance of these observations has not been investigated to the best of our knowledge. Fn1
320 domains and beaded strings in our movies resemble mobile, $Fn1^+$ adhesions similar to those
321 described previously (Lu et al., 2020; Pankov et al., 2000; Zamir et al., 1999; Zamir et al.,
322 2000). The centripetal movement of these adhesions was dependent on the rearward actin
323 flow, and the linkage of Fn1 to actin was mediated by integrin $\alpha5\beta1$ and tensin (Pankov et al.,
324 2000; Zamir et al., 1999; Zamir et al., 2000). Our TIRF microscopy experiments are consistent
325 with these studies and show that integrin $\alpha5\beta1$ co-localizes with the regions of higher Fn1
326 intensity in fibrillar and non-fibrillar adhesions, and that $\alpha5\beta1^+$ focal and fibrillar adhesions are
327 beaded. Taken together, our studies suggest that Fn1 fibrils arise from small mobile
328 nanodomains containing $Fn1^+$ and integrin $\alpha5\beta1^+$ that move toward the cell's center. This

329 centripetal translocation of Fn1 nanodomains is coordinated with their organization into linear
330 arrays, which become longer and longer as more nanodomains are added.
331
332 The number of Fn1 localizations in nanodomains is independent of the antibody type or
333 amount used for staining, indicating that we are using saturating amounts of antibodies.
334 Together with the preservation of the nanodomain architecture upon the treatment with DOC,
335 our studies indicate that the non-uniform, beaded architecture is a salient feature of mature
336 Fn1 fibrils. Two pieces of evidence suggest that Fn1 nanodomains in fibrils are contiguous: 1)
337 the preservation of the linear organization and the nanoarchitecture of Fn1 fibrils after the
338 treatment of cells with DOC which dissolves cell membranes, and 2) the presence of fibrous
339 material between immunogold densities in electron micrographs (Chen et al., 1997; Dzamba
340 and Peters, 1991). The sparsity of Fn1 localizations between Fn1 nanodomains in fibrils
341 indicates that molecules other than or in addition to Fn1 participate in the linking of Fn1
342 nanodomains into strings.
343
344 FUD peptide specifically binds to the N-terminal assembly domain of Fn1 (Maurer et al., 2015;
345 Maurer et al., 2010) and acts as a competitive inhibitor of Fn1-Fn1 interactions (Ma et al.,
346 2015; Tomasini-Johansson et al., 2001). In the absence of FUD, individual fibrils in an
347 established matrix are stable and can be tracked for over 16 hours (data not shown). When
348 FUD is added to cells, it specifically co-localizes with Fn1 fibrils and dismantles the mature Fn1
349 ECM (Filla et al., 2017; Tomasini-Johansson et al., 2001), suggesting that the linear
350 arrangement of Fn1 nanodomains in the fibrillar ECM is maintained through dynamic
351 interactions mediated at least in part by the Fn1 N-terminal assembly domain. Our live imaging
352 experiments demonstrated that in addition to dismantling pre-existing fibrils, FUD effectively
353 blocks their de-novo formation. STORM showed that FUD does not affect the formation of Fn1
354 nanodomains, instead, it blocks the organization of Fn1 nanodomains into linear arrays.

355 Together, these data suggest that FUD may block the dynamic interactions between the N-
356 terminal Fn1 assembly domain and the factor(s) linking Fn1 nanodomains into fibrils.
357
358 The beaded architecture of Fn1 ECM has important implications for the mechanisms of ECM
359 formation, remodeling and signal transduction. The tensile strength of knotted strings is
360 significantly lower than that of strings with uniformly-aligned fibers (Arai et al., 1999; Saitta et
361 al., 1999), thus the beaded architecture of Fn1 fibrils may facilitate their rupture under strain
362 (Ohashi et al., 1999). The non-uniform, nanodomain architecture of Fn1 may facilitate the
363 accessibility of Fn1 fibrils to matrix metalloproteases. In this model, degradation of Fn1 fibrils
364 by metalloproteases may be accomplished by cleaving between Fn1 nanodomains facilitating
365 ECM remodeling. Finally, Fn1 is known to bind growth factors (Martino and Hubbell, 2010;
366 Saunders and Schwarzbauer, 2019; Wijelath et al., 2002), and cell adhesion to ECM is known
367 to orchestrate growth factor signaling (Hynes, 2009). Thus, Fn1 nanodomains could serve as
368 platforms for the binding and presentation of concentrated packets of growth factors to cells,
369 the organization of Fn1 nanodomains into closely-spaced arrays could further facilitate
370 clustering and signaling by growth factor receptors.
371
372 **Acknowledgements**
373 We thank Nathan Astrof for insightful discussions and careful reading of the manuscript,
374 Sydney Astrof for help with data entry and encouragement, Patrick Murphy for endothelial
375 cells, Richard Hynes for the gift of 297.1 antibody, and Tung Chan for help with setting up
376 Western Blotting using ProteinSimple.
377
378 **Sources of Funding** This work was supported by the funding from the National Heart, Lung,
379 and Blood Institute of the NIH R01 HL103920 and R01 HL134935 to SA, by the NIH Office of
380 the Director R21 OD025323-01 to SA, by the pre-doctoral fellowship F31HL151046 to BEA, by

381 the National Institute of General Medicine R35GM122505 to AK, by the National Institute of
382 Arthritis and Musculoskeletal and Skin Diseases R01 AR073236 to JES, by the Faculty Seed
383 Grant from the Center for Engineering MechanoBiology (CEMB), an NSF Science and
384 Technology Center, under grant agreement CMMI: 15-48571. Any opinions, findings, and
385 conclusions or recommendations expressed in this material are those of the authors and do
386 not necessarily reflect the views of the National Science Foundation.

387

388 **Materials and Methods**

389 Materials and Methods are in the Supplemental Methods Word File.

390

391 **Data availability**

392 Reagents generated as a part of this study are available upon request

393

394 **Legends for Figures are included with Figures**

395

396 **Legends for Movies**

397 **Movie 1. Rotational views through the Fn1+ ECM in the cardiac jelly.** Whole E9.5 embryo
398 was stained using rabbit monoclonal anti-Fn1 antibody and imaged using 100x objective, N.A.
399 1.49, with the pinhole set at 0.8 Airy units, and sampling of 40 nm per pixel in x, y. The movie
400 shows 3D reconstruction through 3.4 μm of tissue sampled every 0.121 μm in z. Fn1 is in
401 white, DAPI is in blue. Arrows point to examples of beaded Fn1 fibrils.

402

403 **Movie 2. Fn1 fibrillogenesis imaged by TIRF microscopy.** $Fn1^{mEGFP}$ MEFs were transiently
404 transfected with mCardinal-lifeact, plated on gelatin-coated glass cover slips, and imaged 48
405 hours later. Filming was done every 2 min for 30 min using TIRF and 100x objective, N.A.

406 1.49. The first set shows Fn1-mEGFP channel. Yellow arrows point to centripetally-moving
407 Fn1 nanodomains that appear to be organizing into an elongating linear fibril. The second set
408 is an overlay between Fn1-mEGFP and mCardinal-lifeact.
409
410 **Movie 3. 2% DOC dissolved cytoplasm and nucleus in under 13 min leaving Fn1 fibrils.**
411 MEFs expressing Fn1-mEGFP were plated on glass-bottom slides and labeled with SiRActin
412 (magenta) to visualize F-actin and Hoechst (blue) to visualize DNA. Time lapse was recorded
413 every 54 sec immediately following the addition of DOC solution, pH 8.01, to live cells. The
414 addition of 2% DOC dissolves actin cytoskeleton and nuclei, and leaves Fn1 ECM fibrils
415 (green). Fn1 fibrils collapse following the dissolution of the actin cytoskeleton due to the loss of
416 tension.
417
418 **Movie 4. 3D-rendering of STORM data.** Fn1 fibril underlined in Fig. 4b1 is rotated around the
419 x-axis to show the arrangement of Fn1 localizations in 3D. The movie starts in x-y plane.
420 Yellow arrows point at Fn1 nanodomains in the fibrils. Red arrows point to the space between
421 the nanodomains.
422
423 **Movie 5. Cells incubated with 11-IIIC, show robust fibrillogenesis.** Fn1^{mEGFP} MEFs were
424 plated on glass in 8-well Ibidi chambers for 4 hours, Medium containing 11-IIIC control peptide
425 was then added and cells were filmed every 90 sec for about 15 hours, as described in
426 Methods. The movie begins approximately 30 min after the 11-IIIC-containing medium was
427 added, the time it takes to set up time-laps recording. Arrows point to cell periphery and
428 examples of centripetally moving Fn1 fibrils.
429
430 **Movie 6. FUD interferes with linking centripetally moving Fn1+ nanodomains into fibrils.**
431 Fn1^{mEGFP} MEFs were plated on glass in 8-well Ibidi chambers for 4 hours. Medium containing

432 FUD peptide was then added and cells were filmed every 3 min for about 15 hours, as
433 described in Methods. The movie begins approximately 30 min after the FUD-containing
434 medium was added, the time it takes to set up time-laps recording. Note the dismantling of pre-
435 existing fibrils at the beginning of the movie. Yellow and red arrows point to cell periphery.
436 Note the presence of centripetally moving Fn1-mEGFP “beads” and the scarcity of Fn1 fibrils
437 for the majority of the duration of the movie.
438

References

Arai, Y., Yasuda, R., Akashi, K., Harada, Y., Miyata, H., Kinosita, K., Jr., and Itoh, H. (1999). Tying a molecular knot with optical tweezers. Nature *399*, 446-448.

Chen, Y., Zardi, L., and Peters, D.M. (1997). High-resolution cryo-scanning electron microscopy study of the macromolecular structure of fibronectin fibrils. Scanning *19*, 349-355.

Chernousov, M.A., Faerman, A.I., Frid, M.G., Printseva, O., and Koteliansky, V.E. (1987). Monoclonal antibody to fibronectin which inhibits extracellular matrix assembly. FEBS Lett *217*, 124-128.

Chiang, H.Y., Korshunov, V.A., Serour, A., Shi, F., and Sottile, J. (2009). Fibronectin is an important regulator of flow-induced vascular remodeling. Arterioscler Thromb Vasc Biol *29*, 1074-1079.

Choi, C.K., Vicente-Manzanares, M., Zareno, J., Whitmore, L.A., Mogilner, A., and Horwitz, A.R. (2008). Actin and alpha-actinin orchestrate the assembly and maturation of nascent adhesions in a myosin II motor-independent manner. Nat Cell Biol *10*, 1039-1050.

Choi, M.G., and Hynes, R.O. (1979). Biosynthesis and processing of fibronectin in NIL.8 hamster cells. J Biol Chem *254*, 12050-12055.

Damsky, C.H., Knudsen, K.A., Bradley, D., Buck, C.A., and Horwitz, A.F. (1985). Distribution of the cell substratum attachment (CSAT) antigen on myogenic and fibroblastic cells in culture. J Cell Biol *100*, 1528-1539.

Dzamba, B.J., and Peters, D.M. (1991). Arrangement of cellular fibronectin in noncollagenous fibrils in human fibroblast cultures. J Cell Sci *100 (Pt 3)*, 605-612.

Filla, M.S., Dimeo, K.D., Tong, T., and Peters, D.M. (2017). Disruption of fibronectin matrix affects type IV collagen, fibrillin and laminin deposition into extracellular matrix of human trabecular meshwork (HTM) cells. Exp Eye Res *165*, 7-19.

Fruh, S.M., Schoen, I., Ries, J., and Vogel, V. (2015). Molecular architecture of native fibronectin fibrils. Nat Commun *6*, 7275.

Geiger, B., Bershadsky, A., Pankov, R., and Yamada, K.M. (2001). Transmembrane crosstalk between the extracellular matrix--cytoskeleton crosstalk. Nature reviews Molecular cell biology *2*, 793-805.

Geiger, B., and Yamada, K.M. (2011). Molecular architecture and function of matrix adhesions. Cold Spring Harb Perspect Biol *3*.

Hynes, R.O. (2009). The extracellular matrix: not just pretty fibrils. Science *326*, 1216-1219.

Jimenez, A., Friedl, K., and Leterrier, C. (2020). About samples, giving examples: Optimized Single Molecule Localization Microscopy. Methods *174*, 100-114.

Lu, J., Doyle, A.D., Shinsato, Y., Wang, S., Bodendorfer, M.A., Zheng, M., and Yamada, K.M. (2020). Basement Membrane Regulates Fibronectin Organization Using Sliding Focal Adhesions Driven by a Contractile Winch. Dev Cell *52*, 631-646 e634.

476 Ma, W., Ma, H., and Mosher, D.F. (2015). On-Off Kinetics of Engagement of FNI Modules of
477 Soluble Fibronectin by beta-Strand Addition. PLoS One *10*, e0124941.

478 Martino, M.M., and Hubbell, J.A. (2010). The 12th-14th type III repeats of fibronectin function
479 as a highly promiscuous growth factor-binding domain. FASEB J *24*, 4711-4721.

480 Maurer, L.M., Ma, W., and Mosher, D.F. (2015). Dynamic structure of plasma fibronectin. Crit
481 Rev Biochem Mol Biol *51*, 213-227.

482 Maurer, L.M., Tomasini-Johansson, B.R., Ma, W., Annis, D.S., Eickstaedt, N.L., Ensenberger,
483 M.G., Satyshur, K.A., and Mosher, D.F. (2010). Extended binding site on fibronectin for the
484 functional upstream domain of protein F1 of Streptococcus pyogenes. J Biol Chem *285*,
485 41087-41099.

486 McKeown-Longo, P.J., and Mosher, D.F. (1983). Binding of plasma fibronectin to cell layers of
487 human skin fibroblasts. J Cell Biol *97*, 466-472.

488 Morla, A., Zhang, Z., and Ruoslahti, E. (1994). Superfibronectin is a functionally distinct form of
489 fibronectin. Nature *367*, 193-196.

490 Ohashi, T., Kiehart, D.P., and Erickson, H.P. (1999). Dynamics and elasticity of the fibronectin
491 matrix in living cell culture visualized by fibronectin-green fluorescent protein. Proc Natl Acad
492 Sci U S A *96*, 2153-2158.

493 Pankov, R., Cukierman, E., Katz, B.Z., Matsumoto, K., Lin, D.C., Lin, S., Hahn, C., and
494 Yamada, K.M. (2000). Integrin dynamics and matrix assembly: tensin-dependent translocation
495 of alpha(5)beta(1) integrins promotes early fibronectin fibrillogenesis. J Cell Biol *148*, 1075-
496 1090.

497 Peters, J.H., and Hynes, R.O. (1996). Fibronectin isoform distribution in the mouse. I. The
498 alternatively spliced EIIIB, EIIIA, and V segments show widespread codistribution in the
499 developing mouse embryo. Cell Adhes Commun *4*, 103-125.

500 Rickelt, S., and Hynes, R.O. (2018). Antibodies and methods for immunohistochemistry of
501 extracellular matrix proteins. Matrix Biol *71-72*, 10-27.

502 Rozario, T., Dzamba, B., Weber, G.F., Davidson, L.A., and DeSimone, D.W. (2009). The
503 physical state of fibronectin matrix differentially regulates morphogenetic movements in vivo.
504 Dev Biol *327*, 386-398.

505 Saitta, A.M., Soper, P.D., Wasserman, E., and Klein, M.L. (1999). Influence of a knot on the
506 strength of a polymer strand. Nature *399*, 46-48.

507 Saunders, J.T., and Schwarzbauer, J.E. (2019). Fibronectin matrix as a scaffold for
508 procollagen proteinase binding and collagen processing. Mol Biol Cell *30*, 2218-2226.

509 Schwarzbauer, J.E. (1991). Identification of the fibronectin sequences required for assembly of
510 a fibrillar matrix. J Cell Biol *113*, 1463-1473.

511 Schwarzbauer, J.E., and DeSimone, D.W. (2011). Fibronectins, their fibrillogenesis, and in vivo
512 functions. Cold Spring Harbor perspectives in biology *3*.

513 Sechler, J.L., Rao, H., Cumiskey, A.M., Vega-Colon, I., Smith, M.S., Murata, T., and
514 Schwarzbauer, J.E. (2001). A novel fibronectin binding site required for fibronectin fibril growth
515 during matrix assembly. J Cell Biol *154*, 1081-1088.

516 Sechler, J.L., Takada, Y., and Schwarzbauer, J.E. (1996). Altered rate of fibronectin matrix
517 assembly by deletion of the first type III repeats. J Cell Biol *134*, 573-583.

518 Singh, P., Carraher, C., and Schwarzbauer, J.E. (2010). Assembly of fibronectin extracellular
519 matrix. Annu Rev Cell Dev Biol *26*, 397-419.

520 Singh, P., and Schwarzbauer, J.E. (2014). Fibronectin matrix assembly is essential for cell
521 condensation during chondrogenesis. J Cell Sci *127*, 4420-4428.

522 Skorstengaard, K., Jensen, M.S., Sahl, P., Petersen, T.E., and Magnusson, S. (1986).
523 Complete primary structure of bovine plasma fibronectin. Eur J Biochem *161*, 441-453.

524 Smith, M.L., Gourdon, D., Little, W.C., Kubow, K.E., Eguiluz, R.A., Luna-Morris, S., and Vogel,
525 V. (2007). Force-induced unfolding of fibronectin in the extracellular matrix of living cells. PLoS
526 Biol *5*, e268.

527 Sottile, J., and Chandler, J. (2005). Fibronectin matrix turnover occurs through a caveolin-1-
528 dependent process. Mol Biol Cell *16*, 757-768.

529 Tomasini-Johansson, B.R., Kaufman, N.R., Ensenberger, M.G., Ozeri, V., Hanski, E., and
530 Mosher, D.F. (2001). A 49-residue peptide from adhesin F1 of Streptococcus pyogenes inhibits
531 fibronectin matrix assembly. J Biol Chem *276*, 23430-23439.

532 Tsien, R.Y. (1998). The green fluorescent protein. Annual review of biochemistry *67*, 509-544.

533 Vega, M.E., Kastberger, B., Wehrle-Haller, B., and Schwarzbauer, J.E. (2020). Stimulation of
534 Fibronectin Matrix Assembly by Lysine Acetylation. Cells *9*.

535 Wierzbicka-Patynowski, I., Mao, Y., and Schwarzbauer, J.E. (2004). Analysis of fibronectin
536 matrix assembly. Current protocols in cell biology / editorial board, Juan S Bonifacino [et al]
537 *Chapter 10*, Unit 10 12.

538 Wijelath, E.S., Murray, J., Rahman, S., Patel, Y., Ishida, A., Strand, K., Aziz, S., Cardona, C.,
539 Hammond, W.P., Savidge, G.F.*, et al.* (2002). Novel Vascular Endothelial Growth Factor
540 Binding Domains of Fibronectin Enhance Vascular Endothelial Growth Factor Biological
541 Activity. Circulation research *91*, 25-31.

542 Zamir, E., Katz, B.Z., Aota, S., Yamada, K.M., Geiger, B., and Kam, Z. (1999). Molecular
543 diversity of cell-matrix adhesions. J Cell Sci *112 (Pt 11)*, 1655-1669.

544 Zamir, E., Katz, M., Posen, Y., Erez, N., Yamada, K.M., Katz, B.Z., Lin, S., Lin, D.C.,
545 Bershadsky, A., Kam, Z.*, et al.* (2000). Dynamics and segregation of cell-matrix adhesions in
546 cultured fibroblasts. Nat Cell Biol *2*, 191-196.

547 Zhang, F., Saha, S., and Kashina, A. (2012). Arginylation-dependent regulation of a proteolytic
548 product of talin is essential for cell-cell adhesion. J Cell Biol *197*, 819-836.

549 Zhang, Q., Checovich, W.J., Peters, D.M., Albrecht, R.M., and Mosher, D.F. (1994).
550 Modulation of cell surface fibronectin assembly sites by lysophosphatidic acid. J Cell Biol *127*,
551 1447-1459.

552 Zhang, Q., Magnusson, M.K., and Mosher, D.F. (1997). Lysophosphatidic acid and
553 microtubule-destabilizing agents stimulate fibronectin matrix assembly through Rho-dependent
554 actin stress fiber formation and cell contraction. Mol Biol Cell *8*, 1415-1425.

555 Zhong, C., Chrzanowska-Wodnicka, M., Brown, J., Shaub, A., Belkin, A.M., and Burridge, K.
556 (1998). Rho-mediated contractility exposes a cryptic site in fibronectin and induces fibronectin
557 matrix assembly. J Cell Biol *141*, 539-551.

558 Zhou, X., Rowe, R.G., Hiraoka, N., George, J.P., Wirtz, D., Mosher, D.F., Virtanen, I.,
559 Chernousov, M.A., and Weiss, S.J. (2008). Fibronectin fibrillogenesis regulates three-
560 dimensional neovessel formation. Genes Dev *22*, 1231-1243.
561